arms of the structure by 200 μm, corresponding to s-bend radii of ~60 mm. For these initial experiments two 8 mm-long planar Bragg gratings with periods of 532 and 532.4 nm, respectively, were incorporated into the two arms of each device, resulting in dual-peak spectral responses typical of that shown in Fig. 3. From the graph the distinction between the two grating reflection responses is clear, and future work will be aimed at integrating such gratings into larger optical systems.

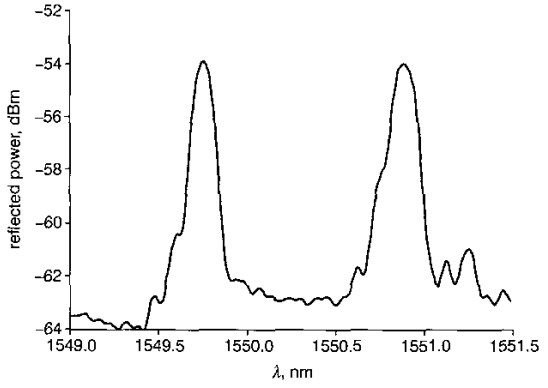

Fig. 3 *Reflection spectra for 2D Mach-Zender channel waveguide structure*

Grating detuning: With the absolute period of our small-spot interference pattern defined by the refractive index of the host material and intersection angle of the two focused beams, the process of centre-wavelength detuning [2] was applied to allow gratings of different periods to be defined via computer-controlled modulation of the writing beam, with no alteration to our optical arrangement. In this detuning process, each stepped exposure of the writing spot is slightly offset from the period of the original interference pattern by a predetermined amount, allowing a selectively different Bragg grating period to be defined in the photosensitive material. While this flexibility comes at an overall loss of grating contrast, an important feature for our direct grating writing process is that the effective wavelength range attainable by detuning is inversely proportional to the number of interference fringes present in the writing spot. In our system a spot diameter of 4 μm with a 532 nm period interference pattern results in approximately eight interference fringes written per exposure. Compared to phase-mask-based schemes, which generally rely on repeated exposures of hundreds of interference fringes, this extremely small writing spot allows a much greater range of detuning from the native interference pattern than traditionally possible. This effect is dramatically demonstrated in the graph of Fig. 4, where an effective detuning range of ~180 nm, encompassing the full S-, C-, and L-wavelength bands, is shown.

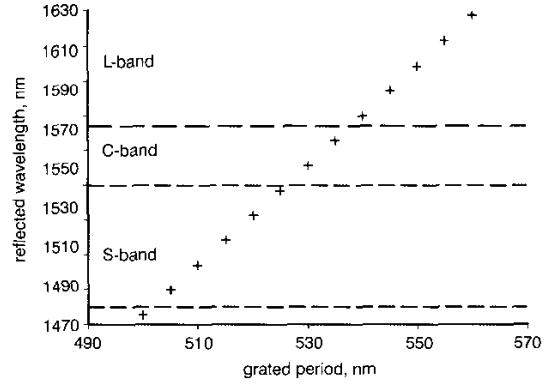

Fig. 4 *Demonstration of grating detuning across S-, C-, and L-wavelength bands*

Conclusion: We have presented two refinements to our recently reported direct grating writing process, each specifically derived from our unique use of a micron-order circular writing spot with an inherent interference pattern. Using these processes, we have demonstrated single-step integration of planar Bragg gratings into 2D Mach-Zender structures and an 180 nm-wide grating detuning response encompassing the S-, C-, and L-wavelength bands, a result achieved entirely through software control. Based on these early results it is hoped that further optimisation of channel waveguide and Bragg grating characteristics will lead to highly efficient integrated optical devices for use in wavelength-selective planar systems.

© IEE 2003
30 May 2003
Electronics Letters Online No: 20030699
DOI: 10.1049/el:20030699

C.B.E. Gawith, G.D. Emmerson, R.B. Williams and P.G.R. Smith (*Optoelectronics Research Centre, University of Southampton, Southampton, SO17 1BJ, United Kingdom*)

E-mail: cbeg@orc.soton.ac.uk

S.G. McMeekin, J.R. Bonar and R.I. Laming (*Alcatel Optronics UK, Starlaw Park, Livingston, EH45 8SF, United Kingdom*)

References

1 SVALGAARD, M., POULSEN, C.V., BJARKLEV, A., and POULSEN, O.: 'Direct UV writing of buried singlemode channel waveguides in Ge-doped silica films', *Electron. Lett.*, 1994, **30**, (17), pp. 1401–1402
2 EMMERSON, G.D., GAWITH, C.B.E., WATTS, S.P., ALBANIS, V., WILLIAMS, R.B., MCMEEKIN, S.G., BONAR, J.R., LAMING, R.I., and SMITH, P.G.R.: 'Photosensitivity locking technique applied to UV written planar Bragg gratings', *Electron. Lett.*, 2003, **39**, (6), pp. 517–518
3 IBSEN, M., DURKIN, M.K., COLE, M.J., and LAMING, R.I.: 'Sinc-sampled fiber Bragg gratings for identical multiple wavelength operation', *IEEE Photonics Technol. Lett.*, 1998, **10**, (6), pp. 842–844

High-speed modulation of 850 nm InGaAsP/InGaP strain-compensated VCSELs

H.C. Kuo, Y.S. Chang, F.Y. Lai, T.H. Hsueh, L.H. Laih and S.C. Wang

High performance 850 nm InGaAsP/InGaP strain-compensated vertical cavity surface emitting lasers (VCSELs) are demonstrated with superior output characteristics and modulation bandwidths up to 12.5 Gbit/s from 25 to 85°C.

Introduction: 850 nm vertical surface emitting lasers (VCSELs) have become a standard technology for application in local area networks (LANs) from 1.25 to 10 Gbit/s [1–4]. The main advantages of VCSELs are the low threshold current, low divergent angle, and circular beam, which lead to simpler packaging and low electrical power consumption. The surface emission from the VCSELs also makes easy the two-dimensional array integration and allows wafer-level testing, in turn leading to low fabrication cost. The use of an Al-free InGaAsP-based active region is an attractive alternative to the conventional (Al)GaAs active region for IR VCSELs; while edge emitting diode lasers with Al-free active regions have demonstrated performance and reliability surpassing AlGaAs-active devices [5]. In addition, theoretical calculations have predicted a lower transparency current density, high differential gain and better temperature performance in InGaAsP-strain active VCSELs compared to lattice-matched GaAs quantum well active devices [6]. These parameters are very important in high-speed and high-temperature applications because the relaxation resonance frequency of the laser depends on the square root of the differential gain as well as the difference of operation current and threshold current [4]. The use of tensile-strained barriers (InGaP) can provide strain compensation and reduce active region carrier leakage. Al-free materials are significantly less reactive to oxide level, which compared to AlGaAs materials makes them ideal for reliable manufacture [5]. Proton-implanted VCSELs using strain $In_{0.18}Ga_{0.82}As_{0.8}P_{0.2}$ active-region has demonstrated good performance [7]. In this Letter, we demonstrate the high-speed and high-

temperature operation of 850 nm oxide-confined VCSELs utilising $In_{0.18}Ga_{0.82}As_{0.8}P_{0.2}/In_{0.4}Ga_{0.6}P$ strain-compensated SC-MQWs.

Structure: The VCSEL shown in Fig. 1 consists of an *n*-type 35-period $Al_{0.15}GaAs/Al_{0.9}Ga_{0.1}As$ distributed Bragg reflector (DBR) grown on a semi-insulating GaAs (100) substrate by a Aixtron 2400G3 metal organic chemical vapour deposition (MOCVD) with growth temperature equal to 750°C. A three-quantum well active region $In_{0.18}Ga_{0.82}As_{0.8}P_{0.2}/In_{0.4}Ga_{0.6}P$ (80 A/100 A) and cladding layer (total 1λ thickness) was then grown, followed by the growth of 22-period $Al_{0.15}GaAs/Al_{0.9}Ga_{0.1}As$ *p*-type mirrors and a 1λ thickness of current spreading layer and thin GaAs contacting layer. The quantum well region growth temperature was set to 650°C. The gain peak = 835 nm was determined by photoluminescence of an angle-etched sample while the FP-dip = 842 nm was determined by reflection measurement. The VCSELs were fabricated utilising the high-speed VCSEL processing to minimise capacitance while keeping reasonably low resistance [3]. The VCSEL has a 5 μm diameter emitting aperture defined by lateral oxidation and Ti/Pt/Au, AuGe/Ni/Au for *p* contact and *n*-metal, respectively.

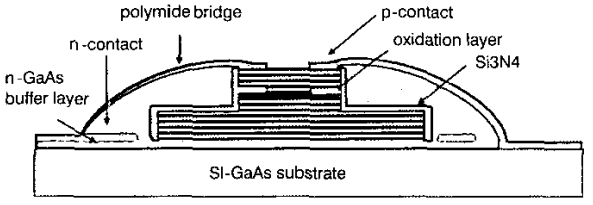

Fig. 1 *Schematic diagram of cross-section of high-speed VCSEL structure*

Results: Fig. 2 shows the typical SC-MQWs InGaAsP/InGaP VCSEL light output and voltage against current (*L–V*) curves over temperature. These VCSELs exhibit kink-free current-light output performance with threshold currents ~0.4 mA, and the slope efficiencies ~0.5 mW/mA. The threshold current change with temperature is <0.2 mA and the slope efficiency drops to <~25% when the substrate temperature is raised from 25 to 90°C. This is superior to the AlGaAs/GaAs VCSEL with similar size [4]. The resistance of our VCSELs is ~95 Ω and capacitance is ~0.1 pF. As a result, the devices are limited by the parasitics to a frequency response of ≃15 GHz.

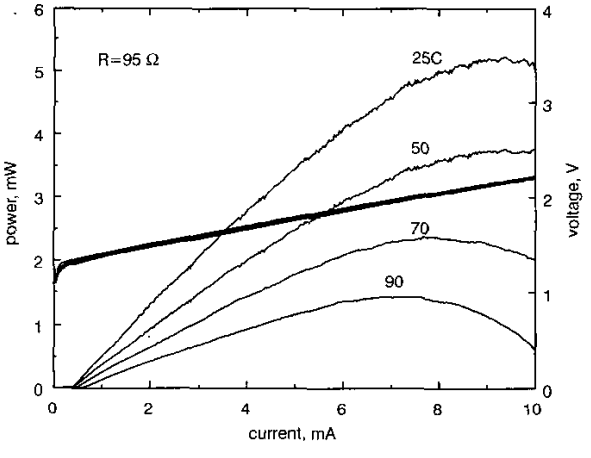

Fig. 2 *SC-MQWs InGaAsP/InGaP VCSEL light output and voltage against current (L–V) curves over temperature*

The small signal response of VCSELs against bias current was measured using a calibrated vector network analyser (Agilent 8720) with on-wafer probing and 50 μm multimode optical fibre connected at a New Focus 25 GHz photodetector. Fig. 3 shows the smoothed small-signal modulation responses of a 5 μm VCSEL at different bias current levels. The modulation frequency is increased with increasing the bias current. With only 3 mA (5 mA) of bias current, the maximum 3 dB modulation frequency response is measured ~13 (14.5) GHz. 14.5 GHz at 25°C, is suitable for 12.5 Gbit/s operation.

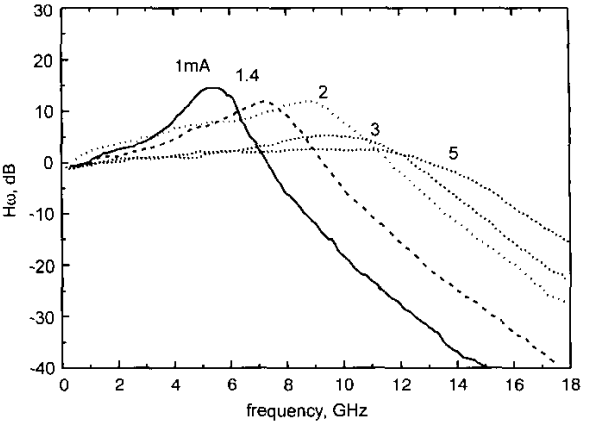

Fig. 3 *Small-signal modulation responses of 5 μm diameter VCSEL at different bias current levels*

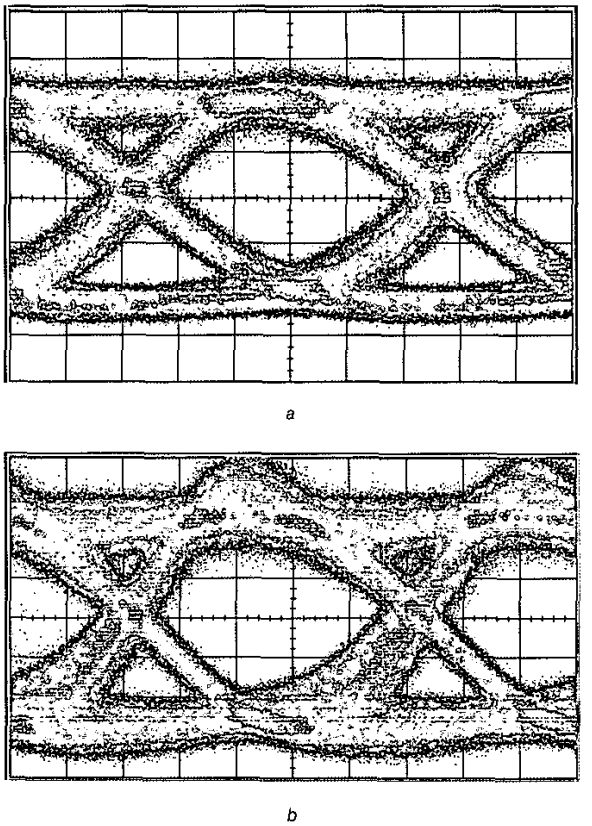

Fig. 4 *Eye diagrams of our VCSEL data up to 12.5 Gbit/s and 6 dB extinction ratio*

a Room temperature eye diagram
b 85°C eye diagram
Scale shown in Fig. is 15 ps/div

To measure the high-speed VCSEL under large signal modulation, microwave and lightwave probes were used in conjunction with a 12.5 Gbit/s pattern generator and a 12 GHz photoreceiver. The eye diagrams were taken for back-to-back (BTB) transmission on an SC-MQWs InGaAsP/InGaP VCSEL. As shown in Fig. 4*a* the room temperature eye diagram of our VCSEL biased at 4 mA with data up to 12.5 Gbit/s and 6 dB extinction ratio has a clear open eye pattern indicating good performance of the VCSELs. The rise time Tr is 28 ps

and fall time Tf is 44 ps with jitter $(p\text{-}p) = 20$ ps. The VCSELs also show superior performance at high temperature. Fig. 4*b* demonstrates the high-speed performance of our VCSEL (biased at 5 mA) with reasonable open eye diagrams at 12.5 Gbit/s and 6 dB extinction ratio at 85°C. This further confirms the superior performance of our VCSEL.

Conclusion: We successfully utilise SC-InGaAsP/InGaP MQWs for fabrication of 850 nm VCSELs with high performance. The VCSELs show very low threshold current, good temperature performance, and high modulation response up to 12.5 Gbit/s from 25 to 85°C.

Acknowledgments: The authors wish to thank G.F. Lin of National Chiao-Tung University, C.P. Kuo and G. Hasnain of LuxNet Corporation, and J.K. Ho of Gigacomm Corporation for useful discussion and technical support. This work is supported by the National Science Council, Republic of China, under contract NSC-90-2215 -E009-088 and by the Academic Excellence Program of the Ministry of Education of the ROC under the contract No. 88-FA06-AB.

© IEE 2003
15 May 2003
Electronics Letters Online No: 20030672
DOI: 10.1049/el:20030672

H.C. Kuo, Y.S. Chang, F.Y. Lai, T.H. Hsueh, L.H. Laih and S.C. Wang (*Institute of Electro-optical Engineering, National Chiao-Tung University, 1001 Ta Hsueh Road, HsinTsu, Taiwan, Republic of China*)

E-mail: hckuo@faculty.nctu.edu.tw

References

1 TATUM, J.A., CLARK, A., GUENTER, J.K., HAWTHORNE, R.A., and JOHNSON, R.H.: 'Commercialization of Honeywell's VCSEL technology' *in* CHOQUETTE, K.D., and LEI, C. (Eds.): 'Vertical-cavity surface-emitting lasers IV', *Proc. SPIE*, SPIE, Bellingham, WA, 2000, **3946**, pp. 2–13
2 PETERS, F.H., and MACDOUGAL, M.H.: 'High-speed high-temperature operation of vertical-cavity surface-emitting lasers', *IEEE Photonics Technol. Lett.*, 2001, **13**, (7), pp. 645–647
3 PETERS, F.H., WELCH, D.J., JAYARAMAN, V., MACDOUGAL, M.H., TAGLE, J.D., GOODWIN, T.A., SCHRAMM, J.E., LOWES, T.D., KILCOYNE, S.P., NARY, K.R., BERGEY, J.S., and CARPENTER, W.: '10 Gb/s VCSEL-based data links', Photonics West, San Jose, CA, USA, Tech. Rep. OE 3946–26, 2000
4 WILMSEN, C.W., TEMKIN, H., and COLDREN, L.A.: 'Vertical-cavity surface-emitting lasers: design, fabrication, characterization, and applications' (Cambridge University Press, 1999)
5 MAWST, L.J., RUSLI, S., AL-MUHANNAWADE, A., and WADE, J.K.: 'Short-wavelength ($0.7\ \mu m < \lambda < 0.78\ \mu m$) high-power InGaAsP-active diode lasers', *IEEE J. Selt. Top. Quantum Electron.*, 1999, **5**, pp. 785–791
6 SALE, T.E., AMAMO, C., OHISO, Y., and KUROKAWA, T.: 'Using strained lasers (AlGa) In As P system materials to improve the performance of 850 nm surface- and edge-emitting lasers', *Appl. Phys. Lett.*, 1997, **71**, pp. 1002–1004
7 TANSU, N., and MAWST, L.J.: 'Compressively-strained InGaAsP-active ($\lambda = 0.85\ \mu m$) VCSELs'. IEEE Lasers and Electro-Optics Society 2000 Annual Mtg (LEOS 2000), Rio Grand, Puerto Rico, 2000, Vol. 2, pp. 724–725

Optimised device processing for continuous-wave operation in GaAs-based quantum cascade lasers

H. Page, S. Dhillon, M. Calligaro, V. Ortiz and C. Sirtori

A significant improvement in the maximum continuous-wave operating temperature of GaAs-based quantum cascade lasers, $T_{max} = 140$ K, is reported. This has been achieved through optimised device processing that significantly reduces the total power consumption of the device and hence its self-heating.

Quantum cascade (QC) lasers are high performance light sources with a very wide emission range ($3.4\ \mu m < \lambda < 80\ \mu m$) [1, 2], based on standard, well characterised semiconductor materials such as GaAs and InP. Routine room temperature continuous-wave (CW) operation of these lasers is an important milestone for a host of applications and a current challenge for the wider dissemination of this technology. Although room temperature CW operation of InP-based QC lasers has been demonstrated [3], reproducing similar performance in GaAs QC devices remains a considerable problem. In this Letter we demonstrate CW operation of a mid-infrared GaAs-based QC laser up to $T_{max} = 140$ K, a substantial improvement on previously published results ($T_{max} = 30$ K) [4], and an important step towards CW operation on electrically cooled elements ($T \sim 240$ K).

The devices presented in this Letter emit at $\lambda \sim 10\ \mu m$ and are based on a GaAs/$Al_{0.45}Ga_{0.55}As$ heterostructure. The design and typical performance characteristics have been published elsewhere [5]. This laser operates routinely at room temperature under low duty cycle pulsed operation (100 ns pulse width at 5 kHz) where self-heating effects are negligible. However, under DC operation, considerable self-heating occurs that can prevent CW operation even at cryogenic temperatures. The source of the self-heating is the large power requirements of the device. The power dissipated in the devices (current × voltage) depends on numerous factors. Above threshold, the voltage is typically 6–8 V, and is related to the number of periods and the emission wavelength. For lasers with 36 periods typical threshold current densities at 77 K are ~3 kA/cm^2. However, the operating current can be minimised, and hence the power requirements, by reducing the area of the laser stripe. For lasers stripes of 2 mm × 20 μm, the power dissipation can be in the range of ~7 to 10 W at 77 K, with a measured thermal resistance of ~6.7 K/W [6]. Taking these characteristics we expect a 56 to 80 K temperature increase in the active region under continuous operation, well within the operating range of the device in pulsed mode (~300 K). Therefore CW operation in these devices should be possible. However, CW operation has not been observed above 30 K [4] because at these power levels other effects, such as thermally induced stresses [3], place a further constraint on the operation of these devices. As shown below, reducing the power requirements further does eventually lead to CW operation.

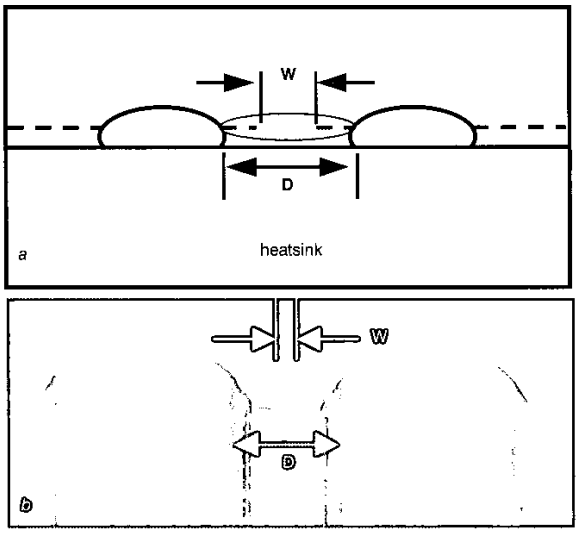

Fig. 1 *Schematic representation of laser facet mounted epilayer down on copper heatsink, and micrograph image of structure*
a Schematic representation *b* Micrograph image

A schematic representation of the laser is given in Fig. 1*a*. First, 600 keV protons are implanted just above the level of the active region (dotted lines). These protons create a zone of defects that compensates the local doping density, thereby rendering the material insulating in this region. Using a suitable mask, an opening of width, W, is left unimplanted to define a current channel to the active region. Two semicircular trenches are wet chemically etched either side, and centred on the channel to define the laser ridge width D ($D > W$). The refractive index contrast offered by the semiconductor air interface at the walls of the ridge strongly confines the optical mode in the lateral